

Application of the Harmonic Control Arrays Technique to Single-Phase Stand-alone Inverters

Mohammad Sadegh Karbasforooshan, Mohammad Monfared, *Senior Member, IEEE*,
and Murat Dogruel, *Senior Member, IEEE*

Abstract—This paper proposes the adaption of the harmonic control array (HCA) technique to control a single-phase stand-alone inverter system. The HCA method is recently proposed as an effective control solution for systems with periodic references or disturbances. The HCA appropriately adjusts the harmonic components of the control signal to obtain a zero steady-state error. Since the signals and parameters involved in this method are complex valued, a discrete time implementation is presented for applying the method through a digital platform. The design procedure of the controller parameters are also presented by details. To confirm the theoretical achievements, experimental results for the prototype system are presented in this paper. The results demonstrate the effectiveness of the suggested control scheme.

Index Terms—Harmonic assembler, harmonic disperser, periodic tracking, discrete time implementation, single-phase stand-alone inverter.

I. INTRODUCTION

STAND-ALONE inverters are widely used in industrial applications to supply sensitive loads or provide electric energy for local loads. So, the main aim of a stand-alone inverter system is to provide a regulated ac voltage, with low total harmonic distortion (THD), in spite of load disturbances and variations, to maintain a high-quality electric power flow to critical/local loads.

The stand-alone inverter system thus requires tracking or rejection of periodic signals. Several control methods to deal with periodic signals have been presented in literature [1-18]. From these, the stationary reference frame proportional resonant (PR) regulator [1-6], the synchronous reference frame (SRF) controller [7-14] and the digital repetitive controller [14-19] have shown successful performance. Although, the PR controller has the advantages of simplicity, low computational burden and zero steady-state error, but this method suffers from exponential decaying response to step changes, high sensitivity to the frequency variations of periodic signals and probability of instability to the phase shift of measured signals [1-6]. The SRF control technique transforms the system variables to a rotating frame at the synchronous speed, where the ac quantities become dc. Therefore, the signal in the SRF can be regulated by a simple proportional integral (PI) controller with zero steady-state error. Among the limitations of the SRF techniques

are the need for several reference frame transformations, which increases the memory requirements and calculation errors, the limited application to balanced systems, complexity of algorithm and etc. [7-14]. Repetitive control which is based on the internal model principle (IMP) is a very useful method that can track or reject periodic signals. The Bode plot of the repetitive controller has infinite amplitudes at multiples of the fundamental frequency that can lead to instability. Although many solutions to solve this problem are presented yet, but this method suffers from other drawbacks, such as a slow transient response, sensitivity to model accuracy and last but not least the high memory requirements [14-19].

The harmonic control array (HCA) method is recently introduced for controlling systems involving periodic reference and/or disturbance signals [20]. The HCA structure automatically constructs the compensating periodic control signal and enables a perfect periodic reference tracking and disturbance rejection. To obtain the harmonic components effectively, HCAs use the running Fourier series integral in its complex nature. Although other control methods may also be utilized in implementing HCAs, an array of proportional integral (PI) controllers is employed in the present paper. The HCA method is easily applicable and effective on periodic tracking or periodic harmonic distortion compensation. In this paper, only brief information is provided for HCAs. Details of description, comparisons with alternative methods and numerical examples can be found in [20].

In this paper, a discrete time implementation procedure for the HCA method is provided so that the required algorithms can be easily and effectively implemented on digital systems. The procedure is applied to a single-phase stand-alone inverter voltage control system. The paper is organized as follows. First, the model of a single-phase stand-alone inverter, with an output LC filter, is described in section II. Then, the basics of the HCA method and its discrete time implementation are summarized in section III. Then, the step-by-step tuning procedure of controller parameters is provided in section IV. Simulation and experiments of the presented system are coming in section V. Finally, the conclusions are drawn in section VI.

II. INVERTER MODEL

The power and control circuits of a single-phase voltage-source stand-alone inverter are shown in Fig. 1. According to

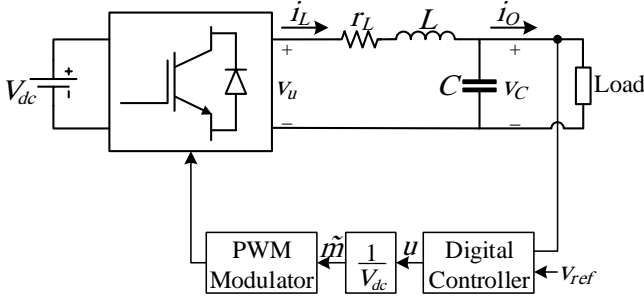


Fig. 1. A voltage-source single-phase stand-alone inverter system: power and control stages.

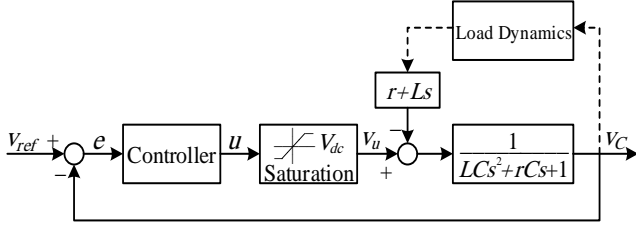


Fig. 2. Block diagram of the control system.

this figure, the power circuit consists of a full-bridge inverter, a LC-type smoothing filter and a local load. The parameters of the system under study are listed in Table 1. The state-space equations of the system can be readily written as (1).

$$\frac{d}{dt} \begin{bmatrix} i_L \\ v_C \end{bmatrix} = \begin{bmatrix} -\frac{r}{L} & -\frac{1}{L} \\ \frac{1}{C} & 0 \end{bmatrix} \begin{bmatrix} i_L \\ v_C \end{bmatrix} + \begin{bmatrix} \frac{1}{L} & 0 \\ 0 & -\frac{1}{C} \end{bmatrix} \begin{bmatrix} v_u \\ i_o \end{bmatrix} \quad (1)$$

Then, the system transfer function is [20]

$$V_C(s) = \frac{1}{LCs^2 + rCs + 1} V_u(s) - \frac{r + Ls}{LCs^2 + rCs + 1} I_o(s). \quad (2)$$

Since the switching frequency of the PWM modulator is chosen to be much higher than the cut-off frequency of the LC low pass filter, then by using the average switching model, one can approximately write

$$v_u \approx \tilde{m} V_{dc} = u. \quad (3)$$

Therefore, the corresponding block diagram of the system is shown in Fig. 2.

III. HARMONIC CONTROL ARRAYS METHOD

Considering a typical system to be feedback controlled, the *Harmonic Control Array* (HCA) structure can be briefly shown as in Fig. 3. Here, r is the reference input, u is the control signal and y is the system output. The other blocks and signals in the diagram are briefly presented in the following subsections.

A. The Harmonic Disperser

A *Harmonic Disperser* (Fig. 4(a)) produces the running harmonic components of the input signal as a function of time. h th *running harmonic* (or simply h th *harmonic*) of a signal $x(t)$ can be obtained using a running Fourier series integral as

TABLE I
SYSTEM PARAMETERS

Parameter	Symbol	Value
dc-link voltage	V_{dc}	250 V
Nominal voltage	V_C	110 Vrms
Nominal power	S	1 kVA
Filter inductance	L	1 mH
Filter capacitance	C	25 μ F
ESR of the inductance	r_L	0.2 Ω
Fundamental frequency	f	60 Hz
Switching frequency	f_s	6 kHz

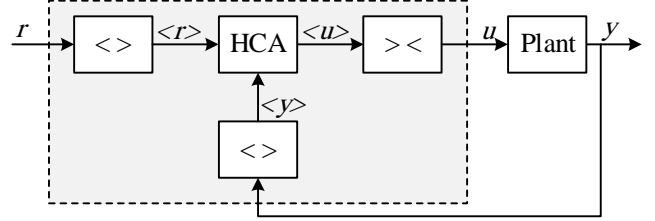


Fig. 3. Harmonic control array block diagram.

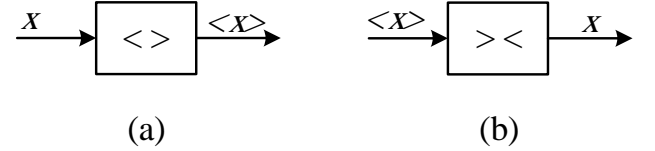


Fig. 4. Harmonic operations: (a) a harmonic disperser and (b) a harmonic assembler.

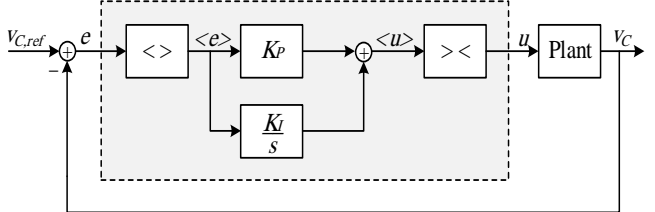


Fig. 5. Harmonic PI control array block diagram.

$$\langle x \rangle_h(t) = \frac{1}{T} \int_{t-T}^t x(\tau) e^{-jh\omega\tau} d\tau \quad (4)$$

where h is an integer number, T represents the fundamental period and it is chosen as a fixed value by the designer and $\omega = 2\pi/T$ is the angular frequency of the reference signal. In our application, $x(t)$ is assumed to be real valued.

$\langle x \rangle_h(t)$ is generally a complex value representing the time-variant Fourier coefficient, also called an $h\omega$ -component lagged running average [8] or a dynamical phasor [22]. Choosing a suitable sampling period by the designer, the Fourier integral of (4) can be calculated in the discrete time by a DSP or a microcontroller. Goertzel algorithm provides an efficient calculation method and saves computation time, as well as storage memory [23]. This technique uses the very last period to correctly assess the harmonic values and to immediately reflect the harmonic changes in the signal. $\langle x \rangle_h$ is closely related to Fourier series coefficients. In fact, if the signal $x(t)$ is actually periodic with T , $\langle x \rangle_h$ will be a complex constant value in time and equal to the h th Fourier series coefficients. Considering harmonic components from 0 to H , the harmonic

dispersion of $x(t)$ can be defined as

$$\langle x \rangle = \begin{bmatrix} \langle x \rangle_0 \\ \langle x \rangle_1 \\ \vdots \\ \langle x \rangle_H \end{bmatrix}. \quad (5)$$

If $\langle x \rangle$ is constant in time (and $x(t)$ does not contain any major harmonic higher than H), then $x(t)$ is periodic with T .

Here, H is a design parameter representing the maximum harmonic number considered. H can be decided according to the process needs and the calculation power of the real platform. If more harmonics are needed to be controlled in the system, then H can be increased, but in this case, the computational load will also increase and a tradeoff may be needed to manage all the calculations in one sampling period. However, with the increasing computational power of DSP devices and the efficient algorithms developed, the feasible implementation of these kinds of operations with high harmonic numbers are becoming possible for even high sampling frequencies.

B. The Harmonic Assembler

A *Harmonic Assembler* (Fig. 4(b)) reconstructs a signal from its running harmonic components. Borrowing from Fourier series synthesis equation, the signal is produced using

$$x(t) = \sum_{h=-H}^H \langle x \rangle_h(t) e^{jh\omega t}. \quad (6)$$

Here, the negative harmonic components are also needed to construct $x(t)$. Since x is assumed to be real valued, $\langle x \rangle_{-h}$ is equal to the conjugate of $\langle x \rangle_h$ (that is $\langle x \rangle_{-h} = \langle x \rangle_h^*$). Therefore, $\langle x \rangle$ as containing the harmonics 0 to H , is sufficient to produce x . From equation 6, an equivalent representation involving only nonnegative harmonics is then

$$x(t) = \langle x \rangle_0(t) + 2\text{Re} \left\{ \sum_{h=1}^H \langle x \rangle_h(t) e^{jh\omega t} \right\}. \quad (7)$$

C. The Harmonic Control Array block

Using $\langle r \rangle$ and $\langle y \rangle$, and possibly their previous values in time, the HCA block in Fig. 3 produces harmonic dispersion of the control signal, $\langle u \rangle$ in an optimum way as much as possible. This can be achieved employing various control methods like linear, fuzzy, sliding mode, adaptive, robust, etc., depending on the designer's choice.

Therefore, the control action works by firstly obtaining the harmonic dispersions of the reference and the system output, then, according to these complex values, the HCA decides on $\langle u \rangle$ and finally the real control input to be applied is composed by a harmonic assembler. There are some complex valued calculations involved in this kind of control; therefore an analog circuit may not be suitable to realize it. Instead, the algorithm can be easily and flexibly implemented on a microcontroller or a DSP. With the higher calculation power and advanced speeds of the digital devices, today it is possible to implement such control algorithms even for relatively fast applications. In the present paper, the HCA block is assumed to be constructed using PI controllers for simplicity. For this case, the corresponding control diagram is as shown in Fig. 5 and, the

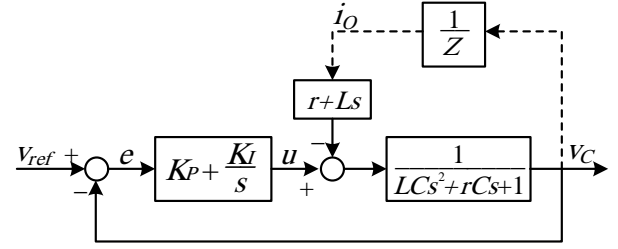


Fig. 6. The simplified block diagram of the single-phase inverter control system.

harmonic dispersion of the control signal is calculated as

$$\langle u \rangle = K_P \langle e \rangle + K_I \int_{-\infty}^t \langle e \rangle dt \quad (8)$$

where $e = r - y$ is the error signal. Note that even if the system is SISO, the dispersion variables will be vectors of dimension $(H+1) \times 1$. Therefore, K_P and K_I are the proportional and integral gain matrices with proper dimensions, and possibly having complex valued entries. In SISO case, these are square matrices with dimension $(H+1) \times (H+1)$. If each harmonic has a feedback only to the same harmonic (which may be suitable for sufficiently linear plants such as our problem), then these gain matrices are diagonal. For nonlinear plants, on the other hand, since the lower harmonics in the plant input may affect the higher harmonics, the off-diagonal entries may be needed for compensation or better control performance. If needed, an *anti-windup* protection algorithm can be used for the integral term in (8). However here, since the values to be integrated are complex numbers in general, the saturation should be activated when the *magnitude* of the integrated complex values are reached to the maximum value foreseen at the design stage.

Instead of only one PI controller as in classical control, an array of PI controllers are, therefore, acting in parallel on each harmonic to compose the final control signal. This, in general, suggests the name “Harmonic Control Array” to describe this kind of control structure.

D. Discrete Time Implementation

As already seen, to use the HCA method, the implementation of the harmonic disperser (4), the HCA block (8) and the harmonic assembler (7) are necessary in the discrete form. To realize these, let use a sampling period of T_s such that $N = T/T_s$ is an integer number. The ratio N/H , as representing the number of points in one sinusoidal period of the highest harmonic, should be as high as possible to get a satisfactory approximation in discrete domain.

The discrete time version of the harmonic disperser of (4) can then be obtained as

$$\langle x \rangle_h[n] = \frac{1}{N} \sum_{k=n-N+1}^n x[k] e^{-jh\omega k T_s} = \frac{1}{N} \sum_{k=n-N+1}^n x[k] e^{-j2\pi h k / N} \quad (9)$$

where $x[k] = x(kT_s)$ and $\langle x \rangle_h[n]$ approximately represents $\langle x \rangle_h(nT_s)$. Note that the exponential term in (9) is a periodic function in time, that is

$$e^{-j2\pi h k / N} = e^{-j2\pi h (k+N) / N}, \quad (10)$$

for each integer k , therefore, it is enough to calculate these terms

for one period (for a total of N cases) only. After recording these values for $k=0, 1, \dots, N-1$, instead of recalculating each time, these values can be called from the memory. Another important calculation time saving can be achieved, noticing that the sum in (9) is carried out for a limited period, and many common terms are present in the addition. To this end, (9) can alternatively be written as

$$\langle x \rangle_h [n] = \langle x \rangle_h [n-1] + \frac{1}{N} (x[n] - x[n-N]) e^{-j2\pi n/N} \quad (11)$$

This last equation, requiring only one complex multiplication, greatly simplifies the calculation load of the harmonic disperser and suggests a feasible way to find the dispersion of the signal $x(t)$ (or $e(t)$) in the discrete time.

The PI HCA block (8) can also be implemented in discrete time using

$$\langle u \rangle [n] = K_p \langle e \rangle [n] + K_I E[n] \quad (12)$$

where E represents the integral of $\langle e \rangle$ in discrete time and can be calculated as

$$E[n] = E[n-1] + T_s \langle e \rangle [n]. \quad (13)$$

To find the real control action u to be applied to the modulator, on the other hand, (7) can be transferred to the discrete domain as

$$u[n] = \langle u \rangle_0 [n] + 2 \operatorname{Re} \left\{ \sum_{h=1}^H \langle u \rangle_h [n] e^{j2\pi h n/N} \right\}. \quad (14)$$

IV. CONTROLLER PARAMETERS DESIGN

The block diagram of the converter in presence of the HCA controller is shown in Fig. 5. It is possible to simplify this model by neglecting the assembler and disperser dynamics and modeling the load dynamics by an impedance Z . Then the controller parameters are designed based on the simplified model shown in Fig. 6.

Traditionally, a very small resistor in series with the filter capacitor is used to passively damp the high-frequency resonances due to switching side-band harmonics, which its effect on the dynamics of the control system can be reasonably neglected.

It is observed that under light loads (Z tends to ∞), the phase margin (PM) and the closed loop stability of the system are decreased [7]. Therefore, the controller is designed and its parameters are tuned under the worst condition; i.e. the no load. As a conservative assumption, this ensures that the system PM will never become smaller than the desired value for a wide range of operating conditions. The simplicity of the controller design is another benefit of neglecting the load dynamics. Under this condition, the plant transfer function simplifies to

$$G_p(s) = \frac{v_c(s)}{u(s)} = \frac{1}{LCs^2 + rCs + 1} \quad (15)$$

and the loop gain is

$$\frac{v_c(s)}{e(s)} = \frac{K_p + K_I/s}{LCs^2 + rCs + 1}. \quad (16)$$

Tuning the PI controller is essentially a tradeoff between the attainable control bandwidth and the loop stability [7]. The

integral part of the PI controller provides a high gain at zero frequency and its effect around the loop cross-over frequency,

and therefore the bandwidth frequency (ω_b), can be neglected, especially in the case of a large bandwidth. So, first it is assumed that $K_I = 0$ and the transfer function of the closed loop system becomes

$$\left. \frac{v_c(s)}{v_{ref}(s)} \right|_{K_I=0} = \frac{K_p}{LCs^2 + rCs + K_p + 1}. \quad (17)$$

Considering -3 dB attenuation for (17) at the bandwidth frequency ω_b yields to

$$\frac{K_p}{\sqrt{(K_p + 1 - LC\omega_b^2)^2 + (rC\omega_b)^2}} = \sqrt{\frac{1}{2}} \quad (18)$$

from which, the proportional gain K_p is calculated as

$$K_p = 1 - LC\omega_b^2 + \sqrt{2(LC\omega_b^2 - 1)^2 + (rC\omega_b)^2}. \quad (19)$$

The control bandwidth of the system in this application is a compromise between the transient response and the switching noise rejection capability, which in this paper is selected to be 1000 Hz. With this selection, a high dynamic performance and at the same time a proper immunity of the control loop to switching noises is ensured. Substituting $\omega_b = 2\pi \times 1000$ rad/s into (19) gives $K_p = 0.32$.

After calculating K_p , based on the selected bandwidth and the filter parameters, the proper value of K_I must be determined according to stability requirements. For this end, the simultaneous effect of K_I and K_p will be considered.

Assuming that the cross-over frequency of the loop gain (16) is close to the closed-loop bandwidth, ω_b , it is possible to examine the stability degree, in terms of the phase margin (PM), from the loop gain (16). Accordingly, the phase of transfer function (16) at ω_b is set equal to $PM - \pi$. The result is shown in (20). To ensure the stable operation of the system, especially in presence of unmodelled dynamics, such as the delays associated to the assembler, disperser and PWM modulator, a PM in the range of $70^\circ - 100^\circ$ is recommended. Evaluating (20) for $PM = 85^\circ$ and $K_p = 0.32$ (already determined), yields $K_I = 101.43$.

$$\tan(PM - \pi) = \frac{\omega_b \left((LK_I - rK_p)C\omega_b^2 - K_I \right)}{K_I^2 + \left(K_p (K_p + 1 - LC\omega_b^2) - rCK_I \right) \omega_b^2} \quad (20)$$

The resulted K_p and K_I are the PI control parameters for the fundamental frequency component. In other words, these parameters are designed for the case $h = 1$. The control parameters for higher harmonics ($h = 3, 5, \dots$) are obtained by dividing K_p and K_I by h .

V. PERFORMANCE EVALUATION

In this section, the experimental results of the prototype system, with the parameters of Table I, are presented. The nominal frequency is 60 Hz and the switching frequency is selected such that f_s/f becomes an integer ($N = 100$). The experimental setup is shown in Fig. 7, which consists of dc-link capacitors fed from a diode rectifier circuit, a full-bridge IGBT

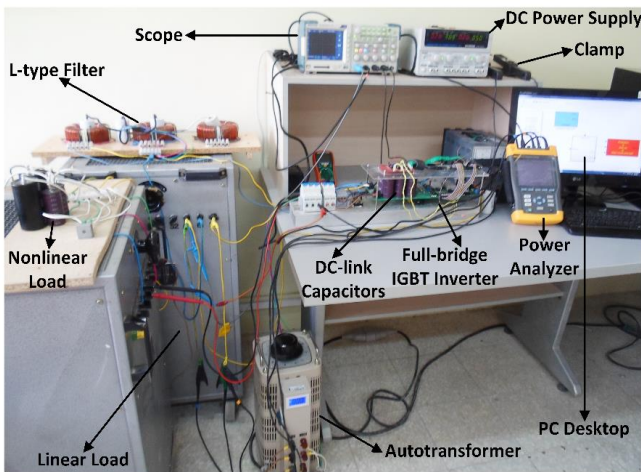


Fig. 7. Experimental setup.

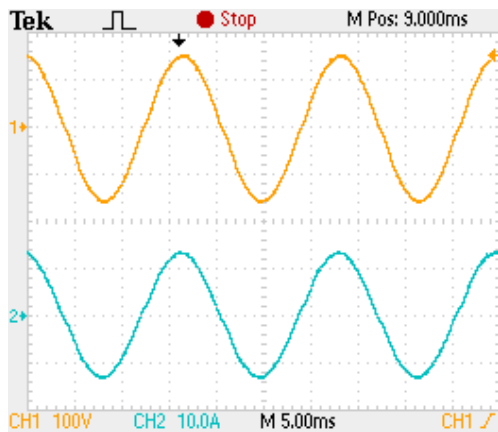


Fig. 8. Steady-state waveforms under nominal resistive load: CH1: output voltage (100 V/div), CH2: load current (10 A/div).

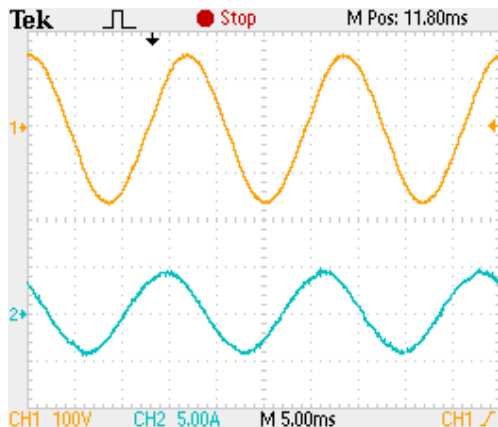


Fig. 9. Steady-state waveforms under RC load: CH1: output voltage (100 V/div), CH2: load current (10 A/div).

inverter, a LC-type output filter and measurement devices. The control algorithm is implemented on a TMS320F28335 digital signal controller from TI.

In the first study, the steady-state performance under the nominal resistive load was examined and the results are shown in Fig. 8. The output voltage waveform is highly sinusoidal with THD = 1.5%. In this test, only the fundamental harmonic component is considered for compensation; i.e. $h = 1$.

In the second study, the experimental results for a capacitive (lightly damped) load is reported in Fig. 9. While the load

power factor (PF) is less than 0.7, the output voltage THD remains below 1.6%. In the final steady-state performance verification, a highly distorted and nonlinear load, according to the IEC 62040-3 standard (Annex E) requirements [24], is connected to the output of the single-phase inverter. The results, when only the fundamental component compensation is included in the control loop ($h = 1$), is shown in Figs. 10 and 11. The THD of the output voltage is 4.2% and the third and fifth harmonics of the output voltage have considerable magnitudes. In the next experiment, the third and fifth harmonics compensation are also added to the control algorithm and the output results for the same loading condition are shown in Figs. 12 and 13. Obviously, the added harmonic compensators can efficiently mitigate the third and fifth harmonics from the output voltage. Then, the output voltage THD is improved to 2.6%, which is far below the standard limit of 8% [24]. However, it is possible to attenuate more harmonics of concern, according to the application requirements, by adding extra HCAs to the controller, at the price of more computation burden. Finally, the transient performance of the system was investigated, with only the fundamental compensation, and the results are depicted in Figs. 14 and 15. In Fig. 14, the transient performance in response to a load step change from no-load to nominal resistive load is shown. The output voltage experiences a small dip at the moment of load connection, which occurs around the voltage peak, and recovers in less than 2 ms. Fig. 15 shows the transient performance of the system in response to a step jump followed by a step fall of the reference voltage magnitude under the nominal resistive load. A slow oscillation, with a very small overshoot/undershoot, can be recognized in the voltage waveform envelope, which safely dies in less than two cycles.

VI. CONCLUSION

This paper proposes the use of HCA method for the single-phase stand-alone inverters. The suggested control method ensures zero steady-state error at the fundamental frequency and other harmonics of interest. This technique takes benefit of a simple concept and ease of implementation on digital platforms. The discrete time implementation of the HCA method along with a systematic procedure to design the control parameters are reported in this paper. The performance of the proposed scheme is confirmed with different experiments. The results indicate the effectiveness and excellent steady-state and transient performance of this method to control the single-phase stand-alone inverter.

REFERENCES

- [1] H. Gholami-Khesht, M. Monfared, and S. Golestan, "Low computational burden grid voltage estimation for grid connected voltage source converter-based power applications," *IET Power Electron.*, vol. 8, no. 5, pp. 656–664, May 2015.
- [2] A. Hasanzadeh, O. C. Onar, H. Mokhtari, and A. Khaligh, "A proportional-resonant controller-based wireless control strategy with a reduced number of sensors for parallel-operated UPSs," *IEEE Trans. Power Deliv.*, vol. 25, no. 1, pp. 468–478, Jan. 2010.
- [3] L. Herman, I. Papic, and B. Blazic, "A proportional-resonant current controller for selective harmonic compensation in a hybrid active power

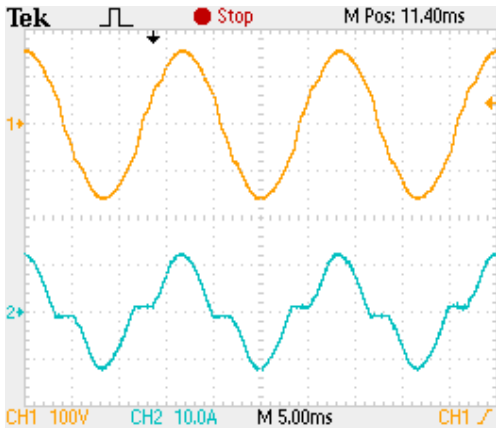


Fig. 10. Steady-state waveforms under highly nonlinear load, including only the fundamental component compensation: CH1: output voltage (100 V/div), CH2: load current (10 A/div).

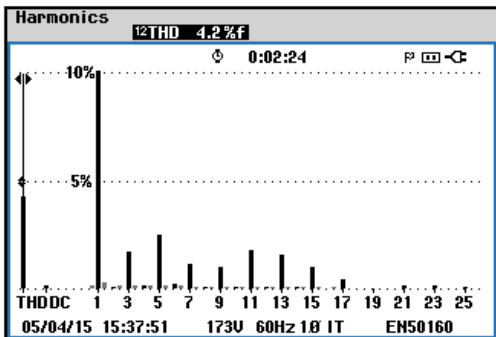


Fig. 11. The harmonic spectrum of the output voltage of Fig. 10.

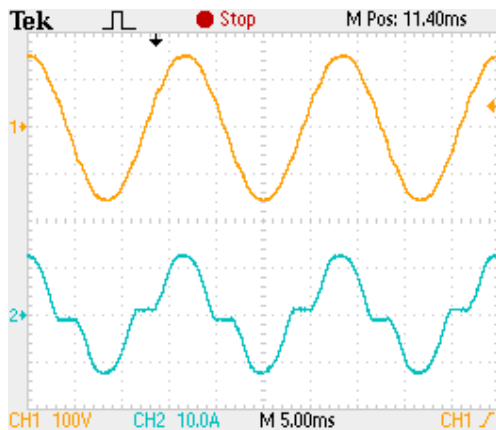


Fig. 12. Steady-state waveforms under highly nonlinear load, including the fundamental and third and fifth harmonics compensation: CH1: output voltage (100 V/div), CH2: load current (10 A/div).

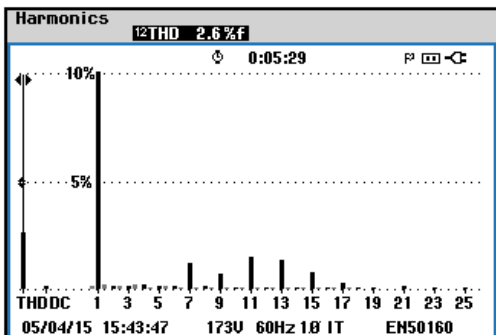


Fig. 13 The harmonic spectrum of the output voltage of Fig. 12.

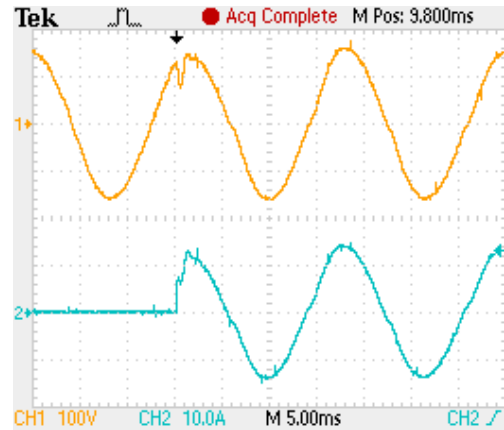


Fig. 14. Transient waveforms in response to no-load to nominal resistive load step change: CH1: output voltage (100 V/div), CH2: load current (10 A/div).

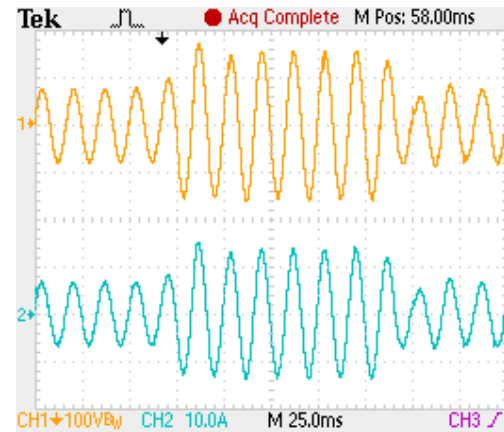


Fig. 15. Transient waveforms in response to +50% followed by -50% step change of reference voltage amplitude: CH1: output voltage (100 V/div), CH2: load current (10 A/div).

- filter," *IEEE Trans. Power Deliv.*, vol. 29, no. 5, pp. 2055–2065, Oct. 2014.
- [4] C. Xia, Z. Wang, T. Shi, and X. He, "An improved control strategy of triple line-voltage cascaded voltage source converter based on proportional-resonant controller," *IEEE Trans. Ind. Electron.*, vol. 60, no. 7, pp. 2894–2908, Jul. 2013.
 - [5] R. Teodorescu, F. Blaabjerg, M. Liserre, and P. C. Loh, "Proportional-resonant controllers and filters for grid-connected voltage-source converters," *IEE Proc. - Electr. Power Appl.*, vol. 153, no. 5, p. 750, 2006.
 - [6] A. Vidal, F. D. Freijedo, A. G. Yepes, P. Fernandez-Comesana, J. Malvar, O. Lopez, and J. Doval-Gandoy, "Assessment and optimization of the transient response of proportional-resonant current controllers for distributed power generation systems," *IEEE Trans. Ind. Electron.*, vol. 60, no. 4, pp. 1367–1383, Apr. 2013.
 - [7] M. Monfared, S. Golestan, and J. M. Guerrero, "Analysis, design and experimental verification of a synchronous reference frame voltage control for single-phase inverters," *IEEE Trans. Ind. Electron.*, vol. 61, no. 1, pp. 258–269, Jan. 2014.
 - [8] P. Mattavelli, "Synchronous-frame harmonic control for high-performance AC power supplies," *IEEE Trans. Ind. Appl.*, vol. 37, no. 3, pp. 864–872, 2001.
 - [9] J. M. Espi Huerta, J. Castello-Moreno, J. R. Fischer, and R. Garcia-Gil, "A synchronous reference frame robust predictive current control for three-phase grid-connected inverters," *IEEE Trans. Ind. Electron.*, vol. 57, no. 3, pp. 954–962, Mar. 2010.
 - [10] A. I. Maswood and F. Liu, "A unity-power-factor converter using the synchronous-reference-frame-based hysteresis current control," *IEEE Trans. Ind. Appl.*, vol. 43, no. 2, pp. 593–599, 2007.
 - [11] R. I. Bojoi, G. Griva, V. Bostan, M. Guerriero, F. Farina, and F. Profumo, "Current control strategy for power conditioners using sinusoidal signal integrators in synchronous reference frame," *IEEE Trans. Power Electron.*, vol. 20, no. 6, pp. 1402–1412, Nov. 2005.

- [12] J. A. Suul, K. Ljokelsoy, T. Midtsund, and T. Undeland, "Synchronous reference frame hysteresis current control for grid converter applications," *IEEE Trans. Ind. Appl.*, vol. 47, no. 5, pp. 2183–2194, Sep. 2011.
- [13] M. Sanatkar-Chayjani and M. Monfared, "Simple digital current control strategy for single-phase grid-connected converters," *IET Power Electron.*, vol. 8, no. 2, pp. 245–254, Feb. 2015.
- [14] C. Zou, B. Liu, S. Duan, and R. Li, "Stationary frame equivalent model of proportional-integral controller in dq synchronous frame," *IEEE Trans. Power Electron.*, vol. 29, no. 9, pp. 4461–4465, Sep. 2014.
- [15] W. Lu, K. Zhou, D. Wang, and M. Cheng, "A generic digital $nk \pm m$ -order harmonic repetitive control scheme for PWM converters," *IEEE Trans. Ind. Electron.*, vol. 61, no. 3, pp. 1516–1527, Mar. 2014.
- [16] G. Escobar, P. G. Hernandez-Briones, P. R. Martinez, M. Hernandez-Gomez, and R. E. Torres-Olguin, "A repetitive-based controller for the compensation of $6l \pm 1$ harmonic components," *IEEE Trans. Ind. Electron.*, vol. 55, no. 8, pp. 3150–3158, Aug. 2008.
- [17] W. Lu, K. Zhou, D. Wang, and M. Cheng, "A general parallel structure repetitive control scheme for multiphase DC–AC PWM converters," *IEEE Trans. Power Electron.*, vol. 28, no. 8, pp. 3980–3987, Aug. 2013.
- [18] K. Zhou, D. Wang, B. Zhang, and Y. Wang, "Plug-in dual-mode-structure repetitive controller for CVCF PWM inverters," *IEEE Trans. Ind. Electron.*, vol. 56, no. 3, pp. 784–791, Mar. 2009.
- [19] Y. Ye, K. Zhou, B. Zhang, D. Wang, and J. Wang, "High-performance repetitive control of PWM DC-AC converters with real-time phase-lead FIR filter," *IEEE Trans. Circuits Syst. II Express Briefs*, vol. 53, no. 8, pp. 768–772, Aug. 2006.
- [20] M. Dogruel, and H. H. Celik, "Harmonic control arrays with a real time application to periodic position control," *IEEE Trans. Control Syst. Technol.*, vol. 19, no. 3, pp. 521–530, May 2011.
- [21] M. Monfared, "A simplified control strategy for single-phase UPS inverters," *Bull. Polish Acad. Sci. Tech. Sci.*, vol. 62, no. 2, pp. 367–373, Jan. 2014.
- [22] S. R. Sanders, J. M. Noworolski, X. Z. Liu, and G. C. Verghese, "Generalized averaging method for power conversion circuits," in *21st Annual IEEE Conference on Power Electronics Specialists*, 1991, pp. 333–340.
- [23] G. Goertzel, "An algorithm for the evaluation of finite trigonometric series," *Am. Math. Mon.*, vol. 65, no. 1, p. 34, Jan. 1958.
- [24] *Uninterruptible power systems (UPS) – Part 3: Method of specifying the performance and test requirements*, Second edition 2011-3, International Standard IEC 62040-3.